Inorganic Chemistry

pubs.acs.org/IC Article

Chemical Information in the L_3 X-ray Absorption Spectra of Molybdenum Compounds by High-Energy-Resolution Detection and Density Functional Theory

Artem Svyazhin,* Vladimir Nalbandyan, Mauro Rovezzi, Aleksandra Chumakova, Blanka Detlefs, Alexander A. Guda, Alessandro Santambrogio, Alain Manceau, and Pieter Glatzel*

Cite This: https://doi.org/10.1021/acs.inorgchem.1c02600 Read Online

ACCESS | Metrics & More | Article Recommendations | Supporting Information

ABSTRACT: X-ray spectroscopy using high-energy-resolution fluorescence detection (HERFD) has critically increased the information content in X-ray spectra. We extend this technique to the tender X-ray range and present a study at the L_3-edge of molybdenum. We show how information on the oxidation state, phase composition, and local environment in molybdenum-based compounds can be obtained by analyzing the HERFD L_3 X-ray absorption near-edge structure (XANES). We demonstrate that the chemical shift of the L_3-edge HERFD spectra follows a parabolic dependence on the oxidation state and show that a qualitative analysis of high-resolution spectra can help to estimate parameters such as distortion of a ligand environment and radial order of atoms around the absorber. In certain cases, the spectra allow disentangling the contributions from bond lengths and angles to the distortion of the ligand polyhedron. Comparison of the high-resolution spectra with theoretical simulations shows that the single-electron approximation is able to reproduce the spectral shape. The results of this work may be useful in every branch of physics, inorganic and organometallic chemistry, catalysis, materials science, biochemistry, and mineralogy where observed changes in performance or chemical properties of Mo-based compounds, accompanied by small changes in spectral shape, are to be related to the details of electronic structure and local atomic environment.

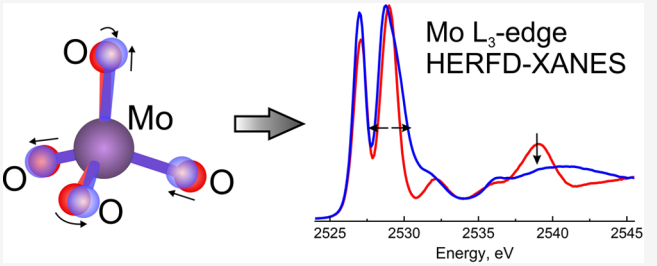

INTRODUCTION

Molybdenum-based compounds find broad application in many fields of science and technology, including catalysis[1−4] and artificial water splitting,[5−8] energy storage and conversion devices,[9−13] and the field of transistor electronics.[14−17] Mo also plays an important role in environmental science[18−21] and in biology, being involved in the nitrogen reduction process.[22,23] X-ray absorption spectroscopy (XAS) is one of the most informative and versatile techniques used for characterization of the oxidation state, symmetry of the local environment, and interatomic distances and is applied widely to Mo compounds. Currently, spectroscopy at the K-edge dominates the spectroscopic investigations of these compounds because hard X-rays do not require vacuum conditions and allow use of different auxiliary devices of any design for *in situ* and *operando* studies. The K-edge also possesses the highest fluorescence yield as compared to any other edge, thus facilitating studies on diluted systems. XAS at the $L_{2,3}$-edges of molybdenum is used less often by the scientific community; however, it has many advantages, which were carefully pointed out by G. N. George[24] and S. J. George[25] and co-workers. With better spectral resolution (1.69 eV at the L_3-edge vs 4.5 eV (K-edge) core hole lifetime broadenings), different Mo species can be resolved which are difficult to determine by other methods.

A crucial advantage of the $L_{2,3}$-edge spectroscopy is that the one-electron selection rules for p-electrons favor studying orbitals of d character, responsible for bond formation for the elements with an open 4d shell, by means of the dipole-allowed $2p \rightarrow 4d$ transitions. In particular, the white lines of the $L_{2,3}$ spectra often reveal a split structure due to crystal field effects. Sensitivity of the white line shape to the crystal field, and, therefore, to the symmetry of the local environment, was successfully applied to the analysis of phase composition and local coordination in many Mo-based compounds.[10,24,26−42] Since EXAFS studies at these edges are impossible due to the vicinity of the $2p_{1/2}$ and $2p_{3/2}$ levels, $L_{2,3}$-edge spectroscopy cannot fully replace the spectroscopic investigations at the K-edge. Nice examples for a complementary K- and L-edge analysis can be found in refs 18, 19, 21, and 43−45.

Received: August 23, 2021

All of the $L_{2,3}$-edge XANES spectra of Mo published so far were collected either in the total fluorescence or electron yield modes. Another approach to the data collection which involves an energy-dispersive spectrometer to choose a preferable decay channel known as high-energy resolution fluorescence-detected (HERFD) XAS[46] has never been applied to the $L_{2,3}$-edges of molybdenum. This method has been gaining increasing popularity over the past decade because of significantly reduced spectral broadening as compared to different conventional yield modes or the transmission measurements, and improved signal-to-noise ratio (see Figure 1; the TFY spectrum was collected simultaneously with the HERFD spectrum using a standard photodiode).[47−49] As applied to the L-edges of molybdenum, the HERFD method helps to resolve the fine structure of the white lines, including direct observation of crystal-field-split 4d states and the shapes of the split manifolds. The structure of the XANES spectra following the white line corresponding to excitations into the continuum of states can also be revealed in greater detail. As will be shown below, qualitative analysis of the Mo L_3-edge XANES measured with high resolution can provide valuable information on the symmetry of the ligand environment, changes in the average Mo−ligand bond lengths, and the radial atomic distribution around the absorber. Using the HERFD method under *operando* conditions can provide insights into the mechanism of chemical reactions, catalysts, or electronic device functioning, or into parameters of chemical bonding of an unknown compound, inaccessible with usual methods of data collection.

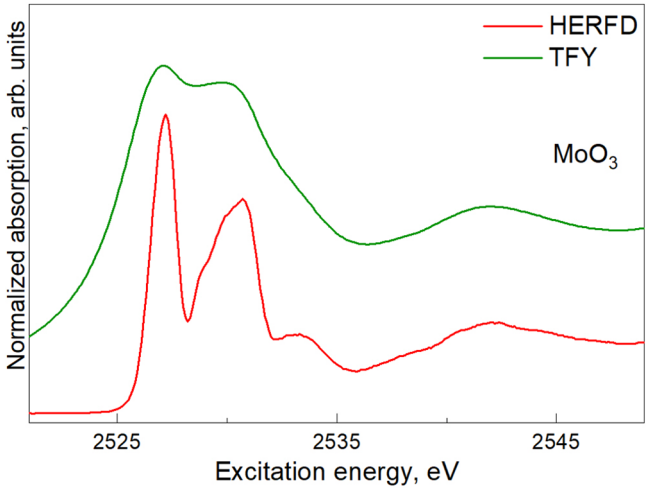

Figure 1. L_3-Edge XANES of MoO_3 obtained by means of total fluorescence yield (TFY) and an Lα_1-detected HERFD spectrum.

If the structure of a compound under investigation is known, the interpretation of the experimental spectra can be performed on the basis of theoretical calculations. Only few publications show simulated Mo $L_{2,3}$ spectra. de Groot et al. and George et al. presented the L-spectra of selected molybdenum references calculated using the multiplet approach.[25,50] Bjornsson et al.[28] simulated L_3-edge XANES of FeMo protein and several model complexes using the ORCA code. Finally, the FEFF9 code was used to simulate the white lines and continuum excitations in a series of Mo reference compounds[51] and catalysts.[52] When it comes to calculations of the XAS at the L-edges of 4d compounds on the basis of single-electron codes, the most debatable question is the strength of multiplet effects at these edges.[28,53,54] For Ru molecular complexes, these effects were suggested to be small, and good results were obtained with single-electron codes.[54,55] There are no similar works for molybdenum compounds yet. Consequently, it is important to establish applicability of single-electron codes to reproduce the experimental Mo L_3-edge spectra, and the high-energy resolution achieved in this work allows for a more detailed comparison with calculations.

We furthermore studied the effect of a core hole potential on the L_3 XANES spectra in Mo compounds in our calculations. In ruthenates, the effect of the core hole in the calculations was found to depend on the type of compounds.[53] There are no similar published works for the compounds of molybdenum. It is important to answer this question because in the case of a weak influence of the core hole potential and negligible multiplet effects the HERFD-XANES at the L_3-edge can be approximated by the orbital momentum projected ground state density of states which greatly facilitates theoretical modeling.

This paper is organized as follows: First, we provide the details of the experiment. Then, we present the experimental HERFD spectra of several reference molybdenum compounds and discuss what information can be extracted from a qualitative analysis of the white lines and the spectral features following them. Next, the results of the ab initio calculations of XANES spectra using Wien2k code[56] of selected compounds are presented, and examples of the analysis of the experimental spectra on the basis of theoretical simulations are given; the role of core hole potential and that of multiplet effects are also discussed in this subsection. Finally, we present the results of calculations carried out by means of the FDMNES code[57] to

Table 1. Parameters of the Local Environment and Oxidation State of Molybdenum in the Investigated Compounds

compound	site symmetry around Mo atom	environment	bond lengths (Å)	formal oxidation state of Mo (valence electron configuration)
Mo metal	O_h	8 Mo	8 × 2.726	0 ($4d^5 5s^1$)
$Mo_2(OAc)_4$	C_1	4 O	2.107, 2.109, 2.121, 2.137	2+ ($4d^4$)
		1 Mo	2.093	
2H-MoS_2	D_{3h}	6 S	6 × 2.417	4+ ($4d^2$)
MoO_2	C_1	6 O	1.968, 1.970, 1.984, 1.990, 2.075, 2.077	4+ ($4d^2$)
		1 Mo	2.512	
MoO_3	C_s	6 O	1.671, 1.734, 2 × 1.948, 2.251, 2.332	
Li_2MoO_4	C_1	4 O	1.76, 1.763, 1.765, 1.77	
Na_2MoO_4	T_d	4 O	4 × 1.771	6+ ($4d^0$)
$CaMoO_4$	S_4	4 O	4 × 1.775	
$ZrMo_2O_8$	C_1	4 O	1.676, 1.733, 1.808, 1.813	

https://doi.org/10.1021/acs.inorgchem.1c02600
Inorg. Chem. XXXX, XXX, XXX−XXX

demonstrate its capabilities as applied to the molybdenum L_3-edge to the potential users; we also discuss the role of the population of the 4d orbitals on the crystal field splitting using this code.

EXPERIMENTAL SECTION

Sample Preparation and Characterization. Samples of MoO_3, Li_2MoO_4, Na_2MoO_4, and $CaMoO_4$ were commercial reagents of analytical grade or higher. Prior to use, they were calcined in air: Li_2MoO_4, Na_2MoO_4, and $CaMoO_4$ at 400 °C and MoO_3 at 600 °C. The high-temperature trigonal form of $ZrMo_2O_8$ was prepared by solid-state reactions from the corresponding reagent-grade oxides. 2H-Molybdenite MoS_2 was an ore concentrate with the only crystalline impurity being quartz. Samples of MoO_2 and $Mo_2(OAc)_4$ were commercial reagents of analytical grade purchased from Sigma-Aldrich. The sample of metallic Mo was a high-quality foil, purchased from Sigma-Aldrich as well. The phase purity of all of the substances was confirmed by powder X-ray diffraction (XRD) using an ARL X'TRA diffractometer and the ICDD's Powder Diffraction File database. The structural parameters of the compounds are presented in Table 1 and Table S1 of the Supporting Information.

Finely ground sample powders were then mixed with boron nitride in 1:1 volume proportion to form 13 mm diameter pellets. No special measures were taken to avoid the self-absorption effect, so the relative intensities of the observed spectral features may differ from those recorded in transmission or total electron yield (TEY) modes or from nanoparticles or single-layered samples. We note that, in many experiments, e.g., carried out *in situ* or *operando*, the particle size corresponds to the thick limit, which for most of the concentrated Mo compounds starts at 2.5 μm (the size of one absorption length for photons of 2.5 keV energy in such compounds). We note that discernible (i.e., >10%) self-absorption effects start already at particle sizes of 100 nm.

HERFD-XANES Measurements. Spectra of the X-ray absorption near-edge structure at the L_3-edge of molybdenum were collected in high-energy-resolution fluorescence-detected (HERFD) mode.[46] The experiments were carried out at beamline ID26 of the European Synchrotron Radiation Facility (Grenoble, France). The incident energy was tuned through the L_3-edge using the (111) reflection of a pair of cryogenically cooled Si crystals. A metallic foil of Mo was used for incident beam energy calibration. The beam footprint on the sample measured 0.1 × 0.7 mm^2, and the total flux was 10^{13} photons/s using the fundamental of three undulators (L = 1.6 m) with 35 mm period. The spectra were obtained with the sample in a vacuum on the TEXS spectrometer, installed on the ID26 beamline of the ESRF synchrotron; the design and performance of the setup are reported elsewhere.[58] For the measurements presented in this work, five Si(111) crystal analyzers with the best bandwidths were picked. The count rate at the top of an absorption spectrum varied from 175.5 × 10^3 for Mo foil to 24.7 × 10^3 c/s for $Mo_2(OAc)_4$. The spectra were normalized to variations of the incoming flux that was recorded by detecting the scattering from a Kapton foil with a photodiode and then were normalized to the same area under the curves within 40 eV above the absorption edge for the purpose of comparison. All of the compounds were checked for radiation damage by making five consecutive XAS scans of 10 s each in the region of the main absorption edge from the same spot on the sample; none of the compounds were found to be radiation-sensitive.

The HERFD-XANES spectra were recorded by monitoring the intensity at the top of the Lα_1 emission line (the $3d_{5/2} \rightarrow 2p_{3/2}$ transition). The relationship between the spectra obtained in the HERFD and conventional XAS modes was discussed elsewhere.[48,59] It was concluded that a HERFD spectrum is a good approximation to the linear absorption coefficient if all absorption features are arranged along diagonals in the full resonant inelastic X-ray scattering (RIXS) plane plotted in the excitation energy vs energy transfer axes. Figure 2 shows the Lα RIXS plane of $ZrMo_2O_8$, typical of the molybdenum compounds investigated in this work. All of the spectral features are running along two diagonal lines corresponding to the $2p^6_{3/2}3d^5_{5/2}$ (full line) and $2p^6_{3/2}3d^5_{3/2}$ (dashed line) final states, split by the 3d spin–orbit coupling. As no off-diagonal resonances are observed on the plane, we conclude that the presented molybdenum L_3-edge HERFD spectra are a good approximation to XAS.

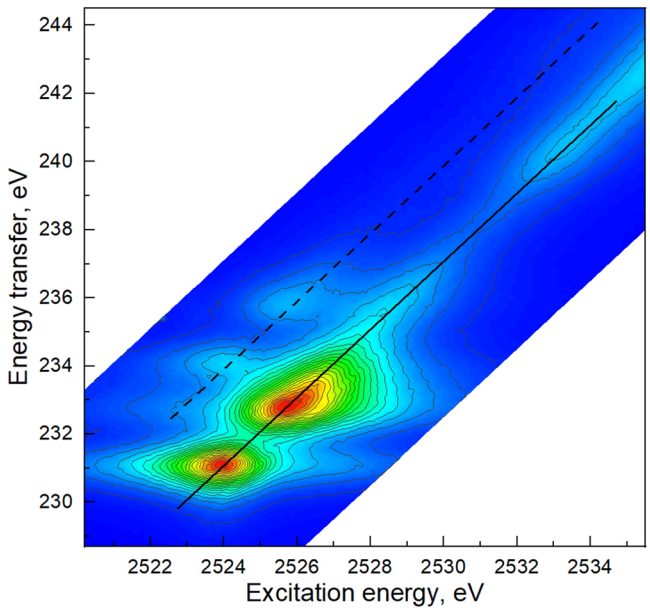

Figure 2. $2p_{3/2}3d$ RIXS plane of $ZrMo_2O_8$. The solid and dashed diagonal lines follow the $3d_{5/2}$ and $3d_{3/2}$ spectral features, respectively.

The origin of the improved experimental broadening characteristic of the HERFD approach was discussed in refs 48 and 60. The overall HERFD energy broadening in our measurements was calculated using the algorithm proposed in ref 48 and is equal to 1.06 eV assuming the Si(111) monochromator resolution to be 0.35 eV at 2.5 keV and the emission spectrometer energy bandwidth to be 1 eV; the widths of the L_3 and M_5 levels were taken from ref 61.

The centroids of the first and second peaks of the white lines of MoO_3, Li_2MoO_4, Na_2MoO_4, $CaMoO_4$, and $ZrMo_2O_8$ were found by means of peak fitting with Gaussian functions and are shown in Figure S1.

Calculations. The Wien2k program package was used for the calculations of the electronic structure and XANES spectra in the ground and excited ($2p^5_{3/2}$ core hole configuration of a Mo atom) states of 2H-MoS_2, MoO_2, and $CaMoO_4$. The Wien2k package was chosen because it is based on the full-potential (linearized) augmented plane-wave + local orbitals method, one of the most accurate schemes for band structure calculations, and the treatment of the core hole potential in this code was proved to be successful in a number of works (see, for example, refs 62–64). We also tested a real-space code for XANES simulations—FDMNES—which can be applied to both periodic solids and molecules: the spectra of metallic molybdenum, molybdenum disulfide, and calcium molybdate were simulated using this package. The details of the calculations and of alignment of the experimental and calculated spectra in each figure are presented in the Supporting Information.

RESULTS AND DISCUSSION

Semiquantitative Analysis of the Experimental L_3-Edge HERFD Spectra. The structural parameters relevant to the local coordination of molybdenum in the compounds under investigation are given in Table 1. Experimental spectra of molybdenum compounds are presented in Figure 3.

The position of the first inflection point (FIP) of the white line shows a monotonic, nonlinear dependence on the formal oxidation state of the Mo ions (Figure 4). The same qualitative pattern was observed by Hedman et al.[65] Nonlinear shifts of

https://doi.org/10.1021/acs.inorgchem.1c02600
Inorg. Chem. XXXX, XXX, XXX−XXX

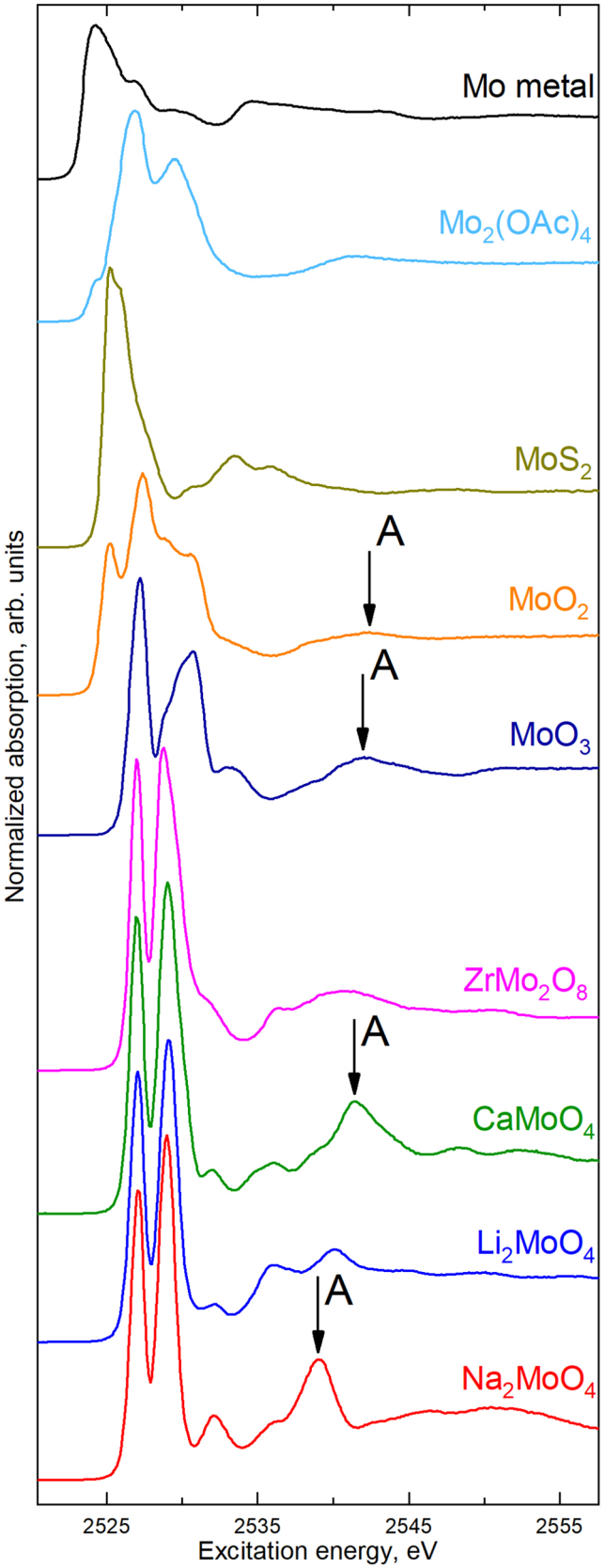

Figure 3. Experimental Mo Lα_1-detected L_3-edge HERFD-XANES spectra of the investigated compounds in the order of increasing formal oxidation state of Mo atoms, from top to bottom. See the text for further details.

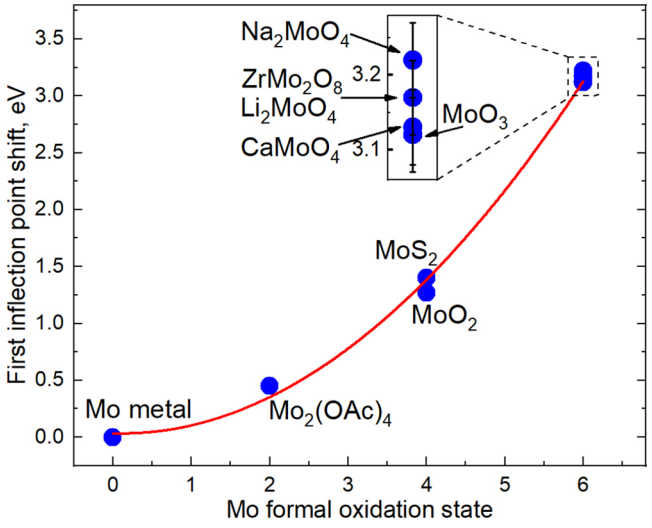

Figure 4. Dependence of the relative position of the first inflection point of the white lines on the formal oxidation state of Mo ions in the investigated compounds. The red line shows a parabolic fit to the experimental points. On the main plot, the full error bar is less than the symbol size.

the Mo $3d_{5/2}$ level with increasing oxidation state were also observed in the XPS experiment.[66] The observed magnitudes of the edge shifts are similar to those measured for the $L_{2,3}$-edge of chromium compounds[67] (chromium is isoelectric to molybdenum). de Groot et al. calculated an alike parabolic dependence for Mo valences from 0 to 6+.[50] In the calculations, the bonding was considered as purely ionic, giving much larger shifts between oxidation states. One can expect considerable deviations from the calculated dependence at higher Mo valences due to the increasingly covalent character of the bonds.[68] However, the rather accurate description by a parabolic fit for both experiment and theory may suggest that covalency does not change much with oxidation state. The zoomed region of the 6+ compounds allows one to conclude that within the experimental error the positions of the FIPs in these compounds depend neither on the number of surrounding ligands nor on the distortion of the O tetrahedron. Thus, according to our results, the experimentally observed shifts of the FIP for a given compound can be attributed to changes in the oxidation state of Mo atoms when coordinated to O, not to changes of a local symmetry.

The characteristic feature of the Mo XANES spectra is a strong white line, corresponding to the $2p^6_{3/2}4d^n \rightarrow 2p^5_{3/2}4d^{(n+1)}$ transition, and a peak A marked with an arrow for some spectra in Figure 3. The white lines are often split into two peaks reflecting the crystal field potential acting on the 4d orbitals resulting in t_{2g} and e_g manifolds for 6-coordinated Mo atoms and t_2 and e for 4-coordinated ones. (In the discussion, we use the same designations for distorted MoO_4 and MoO_6 units for simplicity.) As was demonstrated in the early work by Bare et al., 4-coordinated Mo ions show a characteristic splitting varying from 1.8 to 2.1 eV, and for the sites with six ligands in the first coordination shell, the splitting lies within the 3−4.5 eV range.[29] To quantify the magnitude of the white line splitting in Mo L_3 XANES spectra, the analysis of the second derivative of the absorption spectrum is usually employed,[24] allowing to distinguish easily between the two types of coordination.

https://doi.org/10.1021/acs.inorgchem.1c02600
Inorg. Chem. XXXX, XXX, XXX−XXX

Spectra of all of the compounds, investigated in this work, except for Mo metal, MoO_2, and 2H-MoS_2, reveal well-split white lines (Figure 3). The higher spectral resolution in our data allows for studying details of the energy distribution of the empty d density of states, including direct observation of the split manifolds and the fine peculiarities of an absorption spectrum following the white line. In this context, the group comprising Li_2MoO_4, Na_2MoO_4, $CaMoO_4$, and $ZrMo_2O_8$ is of special interest: Mo atoms are four-coordinated in all of them, and the shape of the MoO_4 units varies from a regular to a strongly distorted tetrahedron. Analysis of the white lines in these compounds with known structure may reveal the capabilities of a qualitative analysis of the L_3-edge HERFD-XANES and will help to illustrate several important points.

The white line region of the spectra is shown in Figure 5, and the most important parameters of the peaks are summarized in Table 2 alongside the relevant parameters of the local environments. The peaks corresponding to the empty states of *e* symmetry show little variations in both full widths at half-maximum (denoted as Γ in Table 2) and the index of asymmetry (IoA), defined as the ratio of the half widths at half height on the low- and high-energy sides of the peak.[69] In contrast, the t_2 peaks reveal significant changes upon reduction of the symmetry of the oxygen tetrahedron in $CaMoO_4$ and $ZrMo_2O_8$ compounds. In terms of molecular symmetry language, the asymmetry of the peaks can be understood as splitting of a 3-degenerate manifold caused by the reduction of the symmetry from cubic. Orbitals of both *e* and t_2 manifolds interact with p orbitals of ligands, but the overlap is stronger for the t_2 orbitals because orbitals of this symmetry point toward the ligands in this type of local environment. Consequently, the latter are more sensitive to the changes of on-site symmetry. The regular tetrahedral environment of Mo in Na_2MoO_4 reveals itself in a perfectly symmetric t_2 peak; in lithium molybdate, deviations of the Mo−O bond lengths and O−Mo−O angles from the regular ones result in growing asymmetry and width of this peak. Further distortions of the oxygen tetrahedron in $CaMoO_4$ and $ZrMo_2O_8$ cause drastic growth in both Γ and IoA of the t_2 peak in these compounds (see Table 2).

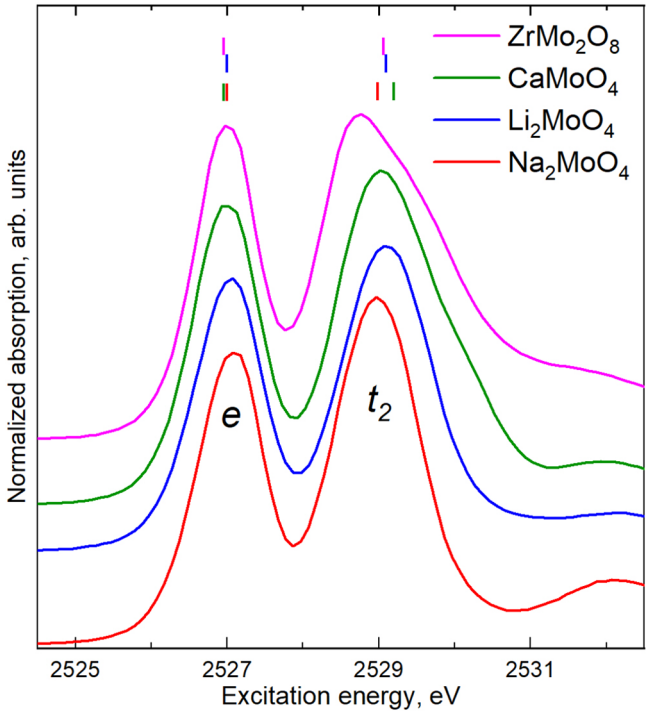

Figure 5. White line region of the Lα_1-detected L_3 HERFD absorption spectra of the compounds with 4-coordinated Mo^{6+} ions. The vertical lines mark centroid positions for each peak of a respective color.

Mo in MoO_3 is in a distorted octahedral environment; therefore, the low-energy peak of the white line corresponds to the empty states of t_{2g} symmetry and the second peak to the empty states of e_g symmetry. Now the e_g orbitals point toward the ligands, showing hence a larger width than the t_{2g} peak. Because of a larger overlap between the d orbitals of Mo and the p orbitals of O, the splitting of the white line is larger than that in 4-coordinated compounds. Significant spread in both bond angles and lengths in MoO_3 results in a very complex shape of the second peak (Figure 3), which must be fitted with at least three Gaussians (see Figure S1). We conclude that in general the shape of the *second* peak of the white line in T_d and O_h environments is more sensitive to the interaction with the ligands and can thus be used for qualitative estimations of the regularity of a ligand polyhedron. Careful analysis of the changes of the second peak, for example, in *operando* studies, can shed light on the mechanism of chemical reactions or functioning of devices based on Mo compounds.

If the manifolds are spectroscopically well-distinguishable, the energy separation between them can be quantified using the difference between the peak maxima ΔE_p or their centroids (ΔE_c) (Table 2), as determined by means of peak fitting. The first approach can be recommended for quick estimations of the type of an environment,[29] because the overlap between the metal d orbitals and p orbitals of a ligand is stronger in the octahedral coordination and the observed splitting of a white line is considerably bigger as compared to that in 4-coordinated compounds. The second procedure provides the

Table 2. Parameters of the Peaks for the Compounds with Well-Split White Lines

compound	O−Mo−O min and max angles[a] (deg)	Mo−O bond lengths (Å)	t_2 (t_{2g}) Γ	t_2 (t_{2g}) IoA	*e* (e_g) Γ	*e* (e_g) IoA	ΔE_p (eV) (±0.01)	ΔE_c (eV) (±0.01)
$ZrMo_2O_8$	106.8, 112.3	1.676, 1.733, 1.808, 1.813	2.00	1.95	1.02	1.08	1.7	2.12
$CaMoO_4$	106.8, 115	4 × 1.775	1.72	1.44	1.09	1.00	2.0	2.25
Li_2MoO_4	107.2, 111.7	1.76, 1.763, 1.765, 1.77	1.43	1.06	1.10	−1.04	2.0	2.11
Na_2MoO_4	4 × 109.47	4 × 1.771	1.36	1.00	1.08	−1.04	1.9	1.98
MoO_3	76.3, 103.8	1.671, 1.734, 2 × 1.948, 2.251, 2.332	1.38	−1.24	3.25	−2.41	3.5	3.1

[a]See the Supporting Information for the details.

https://doi.org/10.1021/acs.inorgchem.1c02600
Inorg. Chem. XXXX, XXX, XXX−XXX

difference in the average energies of the manifolds. In the classic crystal field theory, the interaction between the metal center and the ligands is reduced to the simple electrostatic interaction, and the magnitude of the crystal field splitting is proportional to the Me−ligand bond lengths. Table 2 unambiguously shows that neither ΔE_p nor ΔE_c correlates with Mo−O (average) distances in the 4-coordinated compounds. This point is especially clear for calcium and sodium molybdates, which have comparable nearest neighbor bond lengths but distinctively different ΔE_p and ΔE_c. Asakura et al. have shown theoretically that changes in bond angles may shift centroids of the manifolds even if the bond lengths remain constant.[70] In the ligand field theory which focuses on the construction of molecular orbitals from the orbitals of ligands and the metal center, the energy of an electron is the sum of five components of different signs.[71] Thus, the energy of the splitting of a white line in a crystal field cannot be used for the bond length estimations.

It was suggested previously that the intensity of feature A, which is common for the spectra of all of the compounds investigated in this work (Figures 3 and 6a), correlates with the spread in Mo−ligand bond lengths.[72] This conclusion cannot be confirmed in our investigation. Figures 3 and S2 and Table 1 show unambiguously that despite a bigger difference in the Mo−O bond lengths peak A is more intense in MoO_3 than in MoO_2. Our analysis of the post-white line region of $CaMoO_4$ shows that all of the features in this region result from electron scattering from many coordination shells (CSs), not only from the nearest neighbors. Calculated absorption spectra for the cluster radii RC at which the most important changes in the spectra occur are presented in Figure 6b (the core hole lifetime broadening is not considered). Feature A is already observed at RC = 3 Å, and its shape changes gradually upon increasing the radius of the cluster, converging at RC ≈ 10 Å. Peak C appears at RC = 4.15 Å, and features B and D appear at even larger cluster radii. Whereas intensities of features A, B, and C evolve smoothly, the intensity of feature D jumps up as RC changes from 6.8 to 7.2 Å. We conclude that the shape and intensities of the post-white line spectral features reflect the radial ordering of the atoms around the absorber, which explains the difference in the shapes of peak A in the molybdenum oxides under consideration. In MoO_3, the atoms beyond the oxygen ligands combine into pairs in which atoms are equally distanced from the central Mo atom, whereas, in MoO_2, most of the atoms are distanced (sometimes insignificantly) differently from Mo. (The atomic distributions of atoms around Mo for the molybdenum oxides, $CaMoO_4$ and Na_2MoO_4, are represented graphically in Figure S2.) This implies that the single- and multiple-scattering path lengths contributing to peak A in MoO_2 may be spread almost continuously over some range. Besides that, the types of backscatterers (O and Mo) alternate more randomly in MoO_2 than in MoO_3. These two effects result in a broadening of peak A in MoO_2. $ZrMo_2O_8$ represents a case very similar to MoO_2, and the shapes of peak A in these two compounds are alike.

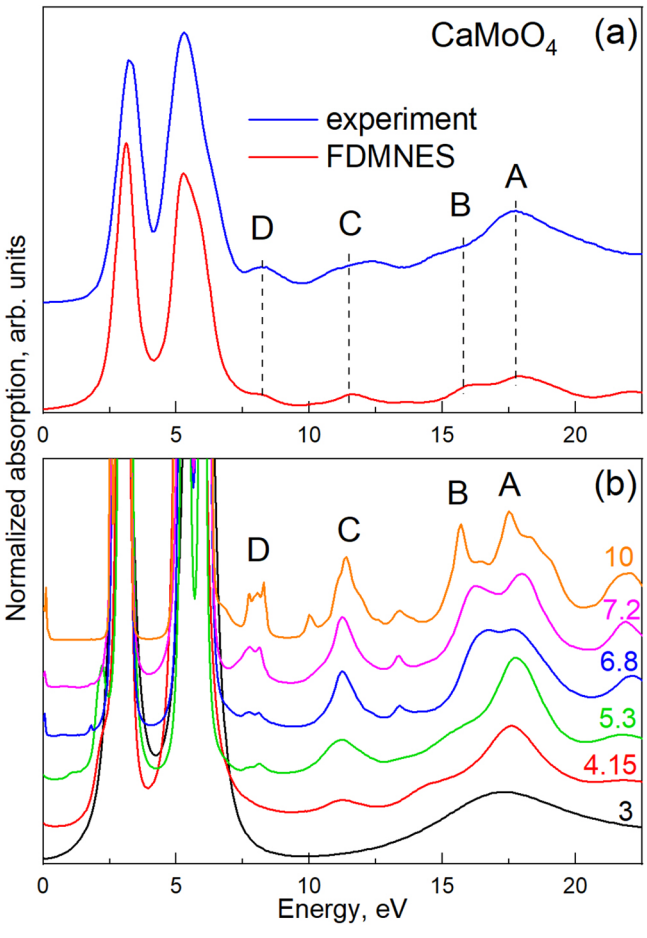

Figure 6. (a) Experimental Lα_1-detected L_3 HERFD and calculated using FDMNES (multiple scattering approach) absorption spectra of $CaMoO_4$. (b) Calculated unconvoluted absorption spectra of $CaMoO_4$ for different cluster radii, whose values (in Å) are indicated above each curve. The dashed vertical lines are the guides to an eye.

The example of the molybdenum oxides proves that a larger spread in the nearest neighbor bond lengths does not necessarily result in a lower radial atomic order. Therefore, there is no straightforward correlation between the Mo−ligand bond lengths and the parameters of peak A. It turns out, however, that, in the compounds with equal Mo−O bond lengths investigated in this work, the atoms beyond the first CS are perfectly ordered over the CSs, and the CSs are distinctly radially separated. As a consequence, the A peaks for $CaMoO_4$ and Na_2MoO_4 are much more intense and narrow as compared to those in the simple oxides. As such, in a spectrum with an asymmetric second white line, a qualitative analysis of the shape of post-edge peak A may help to disentangle the contributions to the distortion of a ligand polyhedron from bond lengths and angles. This can be seen nicely in calcium molybdate where the difference in Mo−O bond angles gives rise to an asymmetric t_2 peak while the equal Mo−O bond lengths cause a sharp and intense peak A.

The position of peak A in different compounds does not correlate with the (average) Mo−O bond lengths (cf. $CaMoO_4$ and Na_2MoO_4, Figure 3 and Table 1). It thus cannot be considered as an analogue to the first continuum resonance in the K-edge XANES. Upon substitution of ligands with atoms of a different sort in a *given compound*, the position of this spectral feature may depend on the average Mo−ligand bond length.[72] This process may be accompanied by changes in the intensity and width of the peak due to the respective changes in the radial ordering of atoms. Consequently, the changes in the position, intensity, and shape of peak A with respect to a reference compound can serve as a marker of ligand substitution, for example, in chemical reactions.

https://doi.org/10.1021/acs.inorgchem.1c02600
Inorg. Chem. XXXX, XXX, XXX−XXX

We summarize the semiquantitative analysis of the Mo L_3-edge:

1. The position of the first inflection point follows a parabolic dependence on the oxidation state. For the group of 6+ compounds with oxygen ligands, within the experimental error, it does not depend on the coordination number and distortions of the O tetrahedron.
2. The white line often shows two distinct groups of excitations that are separated by the crystal field splitting.
3. The magnitude of the peak splitting is indicative of the type of coordination, i.e., 4- or 6-fold coordination.[29]
4. The width and asymmetry of the second white line relates to the regularity of the ligand polyhedron in terms of bond distances and angles.
5. The white line splitting quantified using either peak maxima or centroids does not correlate with the nearest neighbor average bond length.
6. The post-edge peaks become broad with a large spread in nearest neighbor bond distances due to the lowering of radial atomic order. The peaks are rather insensitive to Mo−O bond angles.
7. Peak A may be used to detect changes in bond distances upon ligand substitution in a particular compound.

We note that the presence of several crystallographically and/or chemically inequivalent species may significantly complicate the analysis and even make the conclusions incorrect. The contribution from several inequivalent species, however, is expected to be readily seen in the HERFD spectra.

Wien2k Calculations. Interpretation of the spectral features can be performed based on theoretical calculations. Ideally, the crystal structure of a compound under investigation is known. Codes working in reciprocal space are often the preferred choice in the case of periodic solids, surfaces, and monolayers. 2H-MoS_2 L_3-edge XANES spectra calculated using Wien2k code in the ground state and in the potential of half of an electron and of one electron removed from L_3 core level are presented in the Figure 7. The spectrum calculated for the ground state already reproduces the main features of the experimental spectrum, i.e., the complex structure of the white line peak and a shoulder on its high-energy side. The width of the calculated white line, however, seems to be slightly underestimated. Removal of one core electron results in a collapse of the shoulder and peak splitting. The best agreement with the experimental spectrum in terms of line shape was achieved when taking out half an electron from the L_3 level; i.e., the core hole potential is taken for half a positive charge. Applying half a core hole potential also improves the energy spacing between the white line and the spectral features after it. The features following the white line do not change their relative positions or shapes with the core hole potential owing to the delocalized character of these final states.

To interpret the observed changes in the white line shape upon core hole creation, orbital momentum projected partial densities of states were calculated (Figure 8). The *y* and *z* axes of the local coordinate system were chosen to point along the crystallographic axes *b* and *c* of 2H-MoS_2, respectively, in both single and supercell calculations. The matrix elements for 2p → 5s transitions are 25 times smaller than those for 2p → 4d, and the s-DOS is much smaller than the d-DOS in the white line

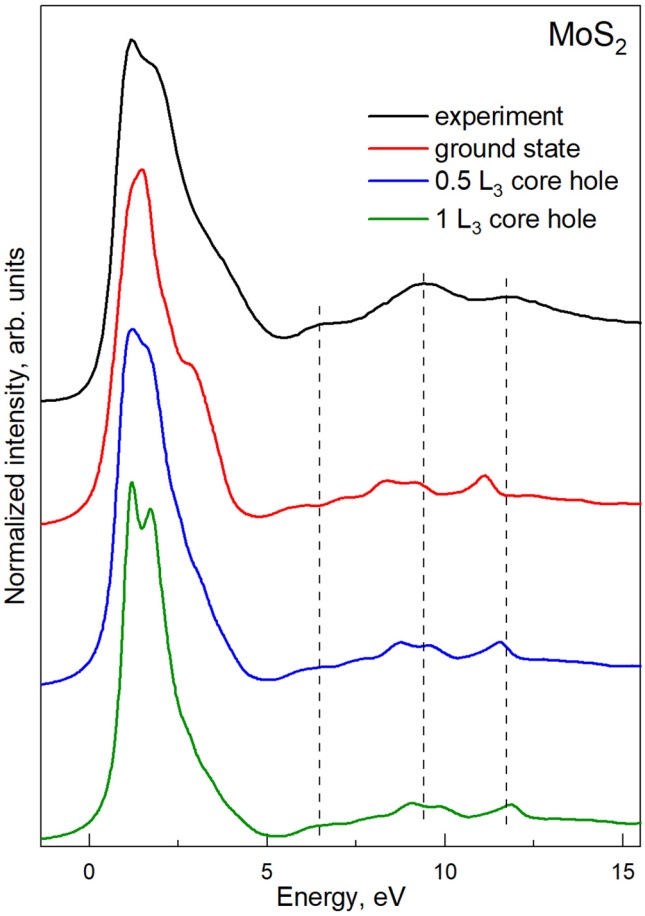

Figure 7. Experimental Lα_1-detected L_3 HERFD and calculated XANES spectra of 2H-MoS_2.

region. We focus therefore in the discussion on the d-DOS only. In the ground state, the d_{z^2} orbital and the double degenerate $d_{x^2-y^2}$ + d_{xy} one are separated from the double-degenerate d_{xz} + d_{yz} orbital by the magnitude of crystal field splitting of 1.2 eV (measured between the centroids of the bands, Figure 8a). As the S^{2-} ion is a weak ligand, the splitting is less than that in 4-coordinated Mo oxides. The splitting does not reveal itself as two peaks in the spectrum because of the significant width of the d_{xz} + d_{yz} band. The unscreened potential of the core hole causes a strong redistribution of the unoccupied states toward the lower energies, resulting in changes of the shape of the white line. Another consequence of the core hole is strong depletion of the d_{xz} + d_{yz} states in the range 3−4.5 eV above the Fermi level (Figure 8b and c), which form the high-energy shoulder in the calculated spectrum.

MoO_2 is a metallic compound in which Mo cations have formal charge 4+. For the calculations of the projected DOS, the local coordinate system proposed by Eyert et al.[73] was adopted. Namely, the *x*-axis was chosen to point along the tetragonal *c*-axis, whereas the *z*-axis is pointing to a corner of the oxygen octahedron. In this local coordinate system, the d_{z^2} and d_{xy} orbitals contribute to the e_g manifold, whereas the $d_{x^2-y^2}$, d_{xz}, and d_{yz} orbitals have t_{2g} symmetry. The calculated partial d-DOS for the ground state is shown in Figure 9a. The admixture of the e_g to t_{2g} states and vice versa, clearly seen in the DOS, can be ascribed to the deviation of the oxygen octahedron from the regular shape. The (d_{xz}, d_{yz}) t_{2g} and (d_{z^2}, d_{xy}) e_g orbitals are split in the crystal field of the surrounding

https://doi.org/10.1021/acs.inorgchem.1c02600
Inorg. Chem. XXXX, XXX, XXX−XXX

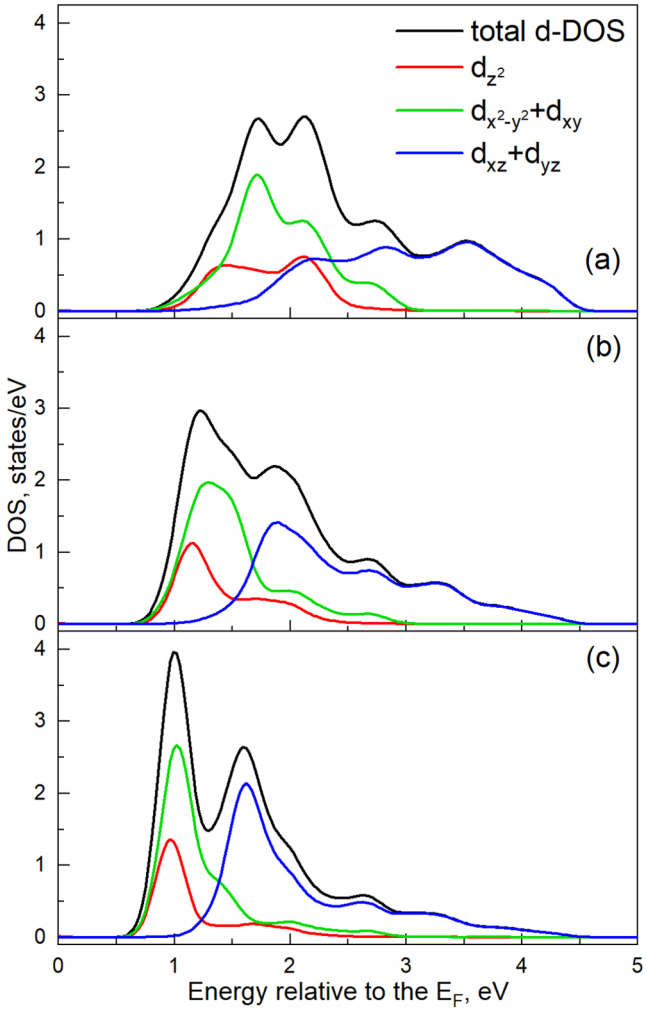

Figure 8. Total and partial Mo DOS in the ground state (a), in the field of 0.5 L_3 core hole potential (b), and full core hole potential (c) for 2H-MoS_2.

oxygen atoms by ~3.5 eV. The $d_{x^2-y^2}$ orbital, which mediates direct Mo−Mo bonding, experiences a strong splitting into bonding and anti-bonding components. The example of MoO_2 demonstrates evidently that a discussion of the shape of a white line in terms of crystal-field-split manifolds is not always possible even for relatively regular environments and that interactions with atoms beyond the first coordination shell may be important.

The XANES for MoO_2 calculated using the ground state DOS does not reveal the double-peak structure observed experimentally (Figure 10). The peaks emerge when half of an electron is removed from the L_3 level. The core hole potential induces changes in the DOS of MoO_2 similar to those in MoS_2. The peaks marked A′, B′, and C′ both in the calculated DOS and XANES in Figures 9b and 10 result from substantial redistribution of the DOS of all of the d orbitals. However, the experimental splitting between A and B is smaller than the distance between A′ and B′. A careful analysis of peak B employing the second derivative shows that its shape is nonuniform and there is a shoulder on its low-energy side (see the inset in Figure 10) which may have an origin similar to C′ in the calculated spectrum. Thus, peak B is likely composed of $d_{x^2-y^2}$, d_{z^2}, and d_{xy} orbitals.

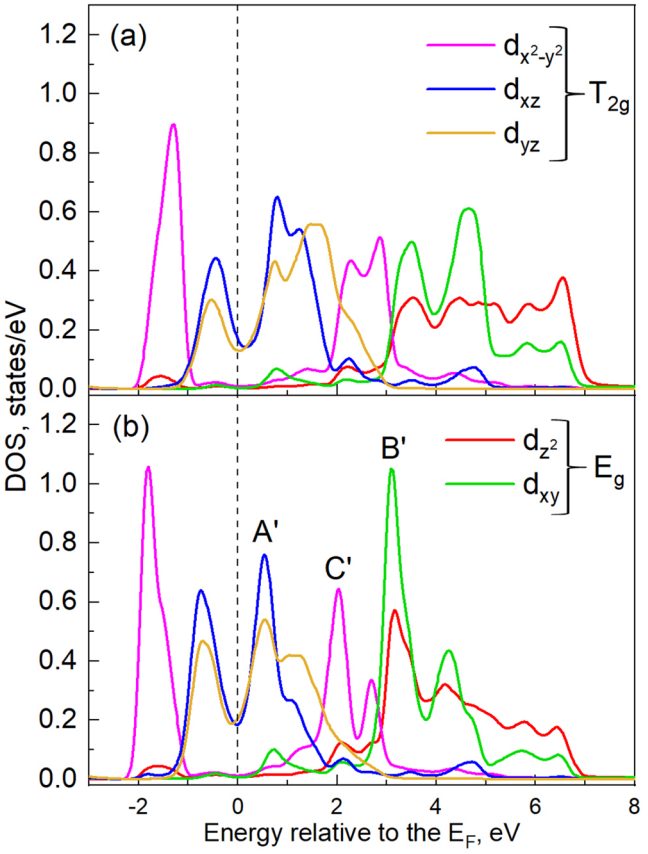

Figure 9. Orbital-resolved DOS of MoO_2 in the ground (a) and in the field of 0.5 core hole (b).

Inclusion of the core hole potential was found to be a prerequisite for getting calculated spectra of a required shape. Another example demonstrating this point in Figure 11 shows calculations with and without the core hole for calcium molybdate. The presence of the core hole improves notably both the shape of the second peak and the t_2/e intensity ratio but reduces the widths of the peaks as compared to the experiment.

The intensities of the ligand-field-split peaks are not simply given by the statistical weight of the unoccupied d orbitals but are influenced by multiplet effects as a result of spin−orbit and intra-atomic electron−electron interactions as well as mixing between Mo and ligand orbitals which may be modified by a core hole potential. Multiplet effects are not fully included in a one-electron density functional theory approach. The calculated t_2/e intensity ratio is smaller than that found experimentally keeping in mind that the experimental ratio is also likely to be reduced somewhat by the effect of self-absorption. Similarly, the calculated B′/A′ peak ratio is smaller than the experimental B/A ratio in MoO_2, and the high-energy side of the calculated spectrum seems to be suppressed. The origin of these discrepancies may be the 2p4d multiplet effects, as they cause spectral weight transfer from the t_{2g} (e) to e_g (t_2) manifolds.[50] It should be noted, however, that the multiplet effects affect the line shapes less significantly than the unscreened core hole potential. As has been shown above, the calculations with the core hole switched on already allow correct discussion of the main spectral features. Thus, we believe that the presented level of agreement between the single-electron theory and experiment is sufficient to discuss

https://doi.org/10.1021/acs.inorgchem.1c02600
Inorg. Chem. XXXX, XXX, XXX−XXX

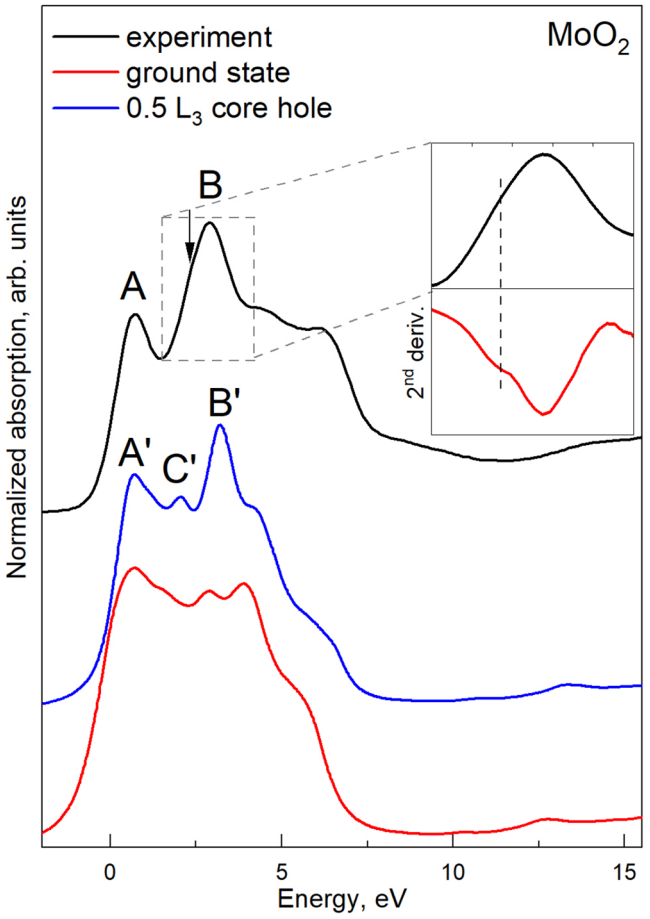

Figure 10. Experimental Lα_1-detected L_3 HERFD and calculated XANES spectra of MoO_2.

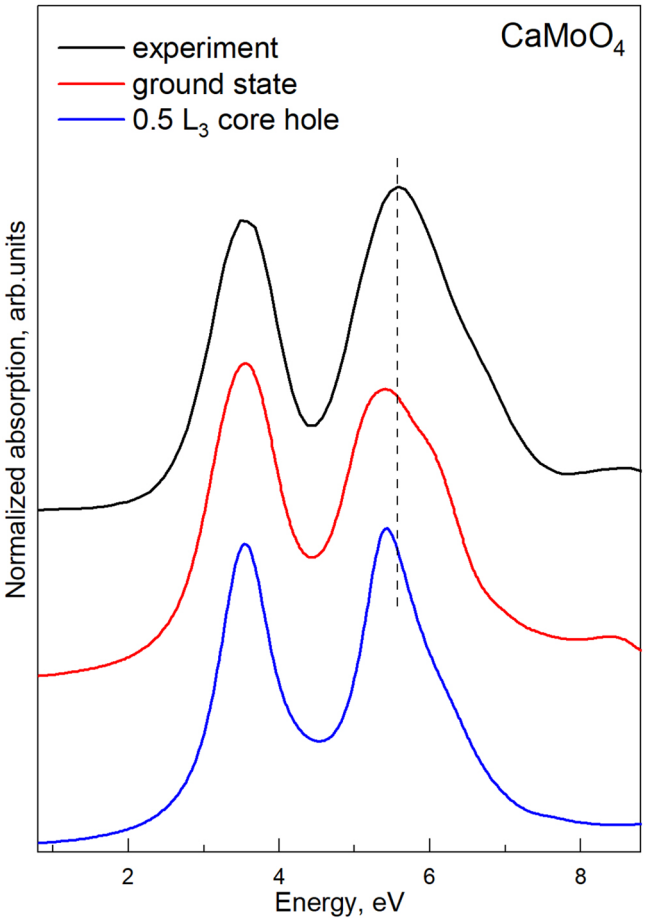

Figure 11. Experimental Lα_1-detected L_3 HERFD and calculated white lines of $CaMoO_4$. The dashed vertical lines are the guides to an eye.

experimentally observed differences among compounds, if only line shapes but not intensities are considered.

Calculations Using FDMNES Code. Reciprocal-space codes can be recommended for the calculations of bulks, surfaces, and monolayered systems. The calculations of molecules and systems with atomic substitutions on the order of a few atomic percent may preferentially be carried out using codes working in the real space. Here, we present the results of calculation of Mo metal, 2H-MoS_2, and $CaMoO_4$ absorption spectra employing FDMNES code to show its abilities in simulation of the Mo L_3-edge XANES and to get a potential user familiar with the most important parameters of the calculations.

The calculated spectra along with the experimental ones are plotted in Figure 12, and the key parameters, or "keywords" using the FDMNES language, which we found to influence the final results most notably are presented in Table S3.

The calculated spectra are in good agreement with the experiment and can be used for an efficient interpretation of experimental data. The spectrum of metallic Mo is predictably well simulated without a core hole due to significant screening of the core hole potential by the delocalized electrons. The spectrum of $CaMoO_4$ (taken from Figure 6a) represents the best compromise among the white line splitting, the shape of the post-white line features, and the energy spacing between them and the white line. We were not able to further improve the correspondence with the experiment for this compound. The white line shape is quite similar to that calculated in Wien2k for the ground state except for the peak splitting, which is larger for FDMNES. One may suspect this difference to originate from different population of the 4d orbitals calculated by the codes. The electrostatic part of the energy of a given orbital on a metal site will obviously decrease upon removal of a part of an electron away from it. Indeed, the population of the d-electrons calculated with Wien2k in the potential of one-half of a core electron hole is 2.76 electrons, whereas that calculated with FDMNES for the spectrum in Figure 12c is 4.26 electrons. Figure 13 unambiguously shows a positive correlation between ΔE_p and the population of 4d orbitals for $CaMoO_4$. We, therefore, conclude that the difference in crystal field splitting calculated using FDMNES and Wien2k code most probably comes from the different numbers of electrons on the 4d orbitals of molybdenum.

SUMMARY AND CONCLUSIONS

High-energy-resolution L_3-edge spectra of molybdenum compounds allow direct experimental observation of the crystal-field-split unoccupied 4d states. The shape of the second peak of a split white line in 4- and 6-fold-coordinated compounds is sensitive to bond angles and distances and thus reflects a distortion of the ligand polyhedron. The intensities and shapes of the spectral features following the white line provide the information on the radial ordering of the atoms around the absorber. Combined analysis of the white line and post-white line features can, in some cases, disentangle

https://doi.org/10.1021/acs.inorgchem.1c02600
Inorg. Chem. XXXX, XXX, XXX−XXX

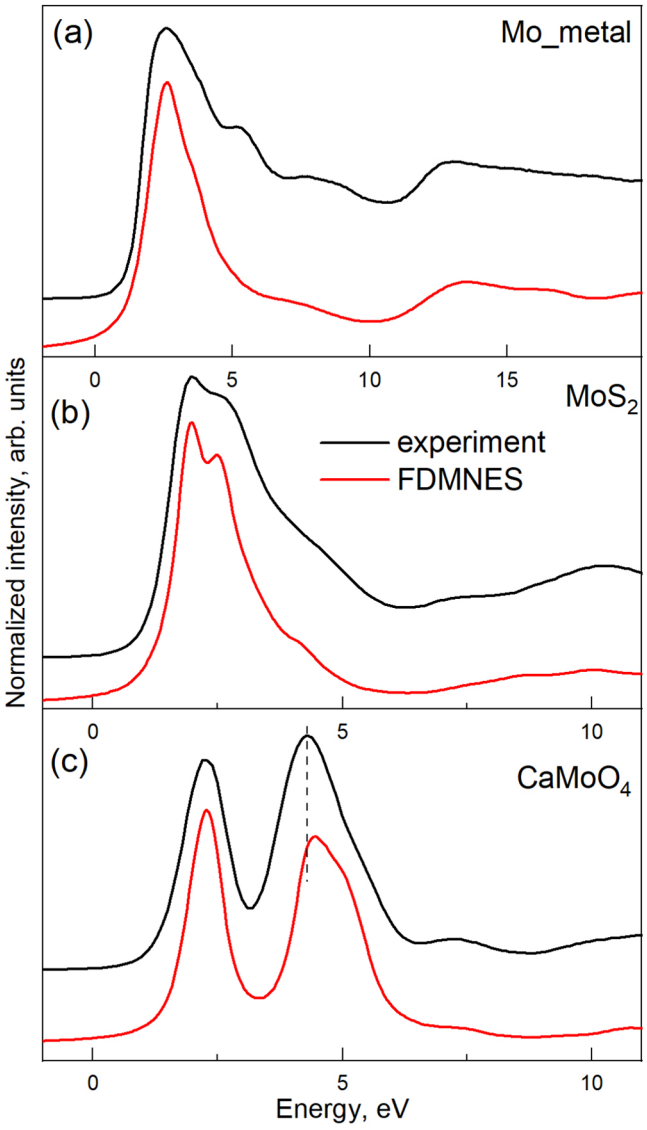

Figure 12. Comparison of the experimental Lα_1-detected L_3 HERFD absorption spectra with calculations using the FDMNES code. The legend from part b is applicable to parts a and c.

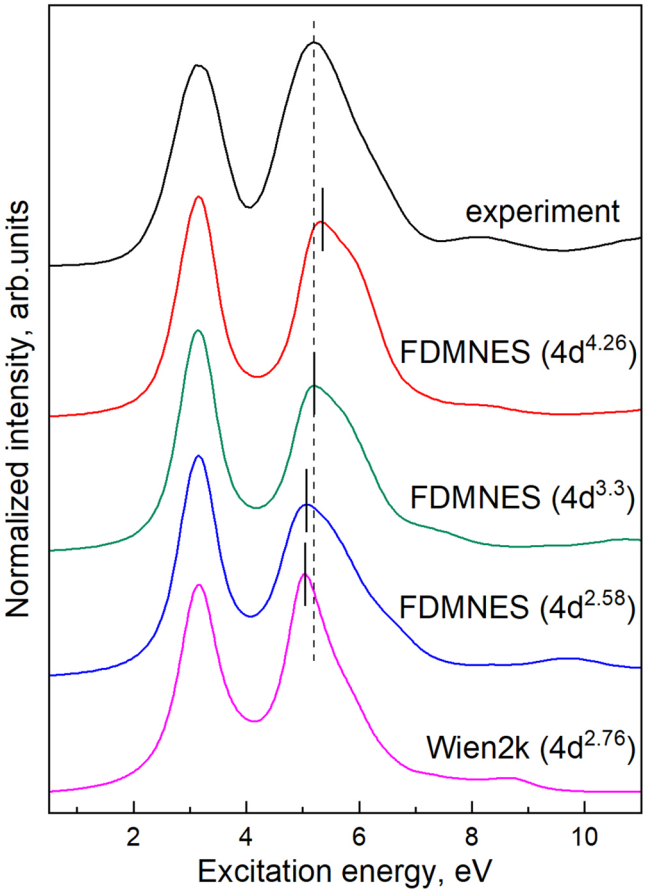

Figure 13. Experimental spectrum and calculated white lines of $CaMoO_4$, corresponding to different populations of the 4d orbitals. The spectrum represented with a red line was taken from Figure 12c. The resulting populations are shown in parentheses above each spectrum. Further details of the calculations can be found in the Supporting Information.

contributions of Mo−O bond angles and bond lengths to the distortion of the oxygen tetrahedron. Changes in the shape and position of peak A with respect to a reference can indicate a ligand substitution around the absorbing atom.

The Wien2k code was shown to be able to reproduce the shape of the experimental spectra well, though the line widths and crystal field splittings are underestimated. We tentatively explain the discrepancy between the experimental and calculated spectra of MoO_2 by 2p4d multiplet effects, which cause transfer of spectral weight from the t_{2g} to e_g orbitals. The same effects are likely responsible for the reduced t_2/e ratio calculated for calcium molybdate. These effects are less important than the core hole potential, which has to be taken into account in calculations to get a good agreement with experiment. The reduced splitting of the white line in this compound is most probably related to the underestimated number of electrons on the 4d orbitals of the Mo atom. Adequate calculated spectra can be obtained using FDMNES code as well; however, an appropriate set of input parameters has to be found for each compound.

The high spectral resolution in HERFD-XANES provides important details on the local electronic structure in Mo compounds that can be used for a stringent assessment of calculations. This is relevant for many applications in materials science where small spectral differences should be detected and explained by modifications of the local structure. Instruments for HERFD-XANES become increasingly available also in the tender X-ray range, making the technique accessible to many researchers.

■ ASSOCIATED CONTENT

Supporting Information

The Supporting Information is available free of charge at https://pubs.acs.org/doi/10.1021/acs.inorgchem.1c02600.

Structural parameters of the Mo references; the results of peak fitting for the 4- and 6-coordinated compounds; details of theoretical calculations; details of alignment of theoretical and experimental spectra in each figure; graphical representation of the radial atomic distribution around the Mo atom in MoO_2, MoO_3, $CaMoO_4$, and Na_2MoO_4; additional information on the calculations presented in Figure 13 (PDF)

https://doi.org/10.1021/acs.inorgchem.1c02600
Inorg. Chem. XXXX, XXX, XXX−XXX

AUTHOR INFORMATION

Corresponding Authors

Artem Svyazhin − *European Synchrotron Radiation Facility, 38043 Grenoble, France; M. N. Mikheev Institute of Metal Physics, Ural Branch of the Russian Academy of Science, 620990 Yekaterinburg, Russia;* orcid.org/0000-0002-6959-5036; Email: art.svyazhin@gmail.com

Pieter Glatzel − *European Synchrotron Radiation Facility, 38043 Grenoble, France;* orcid.org/0000-0001-6532-8144; Email: glatzel@esrf.fr

Authors

Vladimir Nalbandyan − *Chemistry Faculty, Southern Federal University, Rostov-on-Don 344090, Russia;* orcid.org/0000-0002-8624-0165

Mauro Rovezzi − *Université Grenoble Alpes, CNRS, IRD, Irstea, Météo France, OSUG, FAME, 38000 Grenoble, France;* orcid.org/0000-0003-2539-6198

Aleksandra Chumakova − *European Synchrotron Radiation Facility, 38043 Grenoble, France*

Blanka Detlefs − *European Synchrotron Radiation Facility, 38043 Grenoble, France*

Alexander A. Guda − *The Smart Materials Research Institute, Southern Federal University, 344090 Rostov-on-Don, Russia;* orcid.org/0000-0002-6941-4987

Alessandro Santambrogio − *European Synchrotron Radiation Facility, 38043 Grenoble, France;* orcid.org/0000-0003-3406-9658

Alain Manceau − *Université Grenoble Alpes, CNRS, ISTerre, CS 40700, 38058 Grenoble, France;* orcid.org/0000-0003-0845-611X

Complete contact information is available at: https://pubs.acs.org/10.1021/acs.inorgchem.1c02600

Notes

The authors declare no competing financial interest.

ACKNOWLEDGMENTS

We acknowledge the European Synchrotron Radiation Facility for provision of synchrotron radiation facilities. A.Sv. acknowledges the state assignment of Ministry of Science and Higher Education of the Russian Federation (theme "Electron" No. AAAA-A18-118020190098-5). A.A.G. acknowledges the financial support by the Ministry of Science and Higher Education of the Russian Federation (State assignment in the field of scientific activity, No. 0852-2020-0019). A.Sv. dedicates this paper to his mother, who passed away untimely during preparation of the manuscript.

REFERENCES

(1) Duyar, M. S.; Tsai, C.; Snider, J. L.; Singh, J. A.; Gallo, A.; Yoo, J. S.; Medford, A. J.; Abild-Pedersen, F.; Studt, F.; Kibsgaard, J.; Bent, S. F.; Nørskov, J. K.; Jaramillo, T. F. A Highly Active Molybdenum Phosphide Catalyst for Methanol Synthesis from CO and CO2. *Angew. Chem.* **2018**, *130*, 15265−15270.

(2) Shen, Y.; Jiang, P.; Wai, P.; Gu, Q.; Zhang, W. Recent Progress in Application of Molybdenum-Based Catalysts for Epoxidation of Alkenes. *Catalysts* **2019**, *9*, 31.

(3) Yao, K.; Yuan, Z.; Jin, S.; Chi, Q.; Liu, B.; Huang, R.; Zhang, Z. Efficient hydrodeoxygenation of sulfoxides into sulfides under mild conditions using heterogeneous cobalt-molybdenum catalysts. *Green Chem.* **2020**, *22*, 39−43.

(4) Tang, C.; Jiao, Y.; Shi, B.; Liu, J.; Xie, Z.; Chen, X.; Zhang, Q.; Qiao, S. Coordination Tunes Selectivity: Two-Electron Oxygen Reduction on High-Loading Molybdenum Single-Atom Catalysts. *Angew. Chem., Int. Ed.* **2020**, *59*, 9171−9176.

(5) Li, J.-S.; Wang, Y.; Liu, C.-H.; Li, S.-L.; Wang, Y.-G.; Dong, L.-Z.; Dai, Z.-H.; Li, Y.-F.; Lan, Y.-Q. Coupled molybdenum carbide and reduced graphene oxide electrocatalysts for efficient hydrogen evolution. *Nat. Commun.* **2016**, *7*, 11204.

(6) Li, H.; Chen, S.; Jia, X.; Xu, B.; Lin, H.; Yang, H.; Song, L.; Wang, X. Amorphous nickel-cobalt complexes hybridized with 1T-phase molybdenum disulfide via hydrazine-induced phase transformation for water splitting. *Nat. Commun.* **2017**, *8*, 15377.

(7) Huang, Y.; et al. Atomically engineering activation sites onto metallic 1T-MoS2 catalysts for enhanced electrochemical hydrogen evolution. *Nat. Commun.* **2019**, *10*, 982.

(8) Ben-Naim, M.; Britto, R. J.; Aldridge, C. W.; Mow, R.; Steiner, M. A.; Nielander, A. C.; King, L. A.; Friedman, D. J.; Deutsch, T. G.; Young, J. L.; Jaramillo, T. F. Addressing the stability gap in photoelectrochemistry: Molybdenum disulfide protective catalysts for tandem III-V unassisted solar water splitting. *ACS Energy Letters* **2020**, *5*, 2631−2640.

(9) Tsai, M. L.; Su, S. H.; Chang, J. K.; Tsai, D. S.; Chen, C. H.; Wu, C. I.; Li, L. J.; Chen, L. J.; He, J. H. Monolayer MoS2 heterojunction solar cells. *ACS Nano* **2014**, *8*, 8317−8322.

(10) Song, H.; Jeong, T.-G.; Moon, Y. H.; Chun, H.-H.; Chung, K. Y.; Kim, H. S.; Cho, B. W.; Kim, Y.-T. Stabilization of Oxygen-deficient Structure for Conducting Li4Ti5O12-δ by Molybdenum Doping in a Reducing Atmosphere. *Sci. Rep.* **2015**, *4*, 4350.

(11) Chen, C. J.; Yang, K. C.; Liu, C. W.; Lu, Y. R.; Dong, C. L.; Wei, D. H.; Hu, S. F.; Liu, R. S. Silicon microwire arrays decorated with amorphous heterometal-doped molybdenum sulfide for water photoelectrolysis. *Nano Energy* **2017**, *32*, 422−432.

(12) Singh, E.; Kim, K. S.; Yeom, G. Y.; Nalwa, H. S. Atomically thin-layered molybdenum disulfide (MoS2) for bulk-heterojunction solar cells. *ACS Appl. Mater. Interfaces* **2017**, *9*, 3223−3245.

(13) Panda, M. R.; Raj, K. A.; Ghosh, A.; Kumar, A.; Muthuraj, D.; Sau, S.; Yu, W.; Zhang, Y.; Sinha, A.; Weyland, M.; Bao, Q.; Mitra, S. Blocks of molybdenum ditelluride: A high rate anode for sodium-ion battery and full cell prototype study. *Nano Energy* **2019**, *64*, 103951.

(14) Yoon, Y.; Ganapathi, K.; Salahuddin, S. How good can monolayer MoS2 transistors be? *Nano Lett.* **2011**, *11*, 3768−3773.

(15) Das, S.; Chen, H. Y.; Penumatcha, A. V.; Appenzeller, J. High performance multilayer MoS2 transistors with scandium contacts. *Nano Lett.* **2013**, *13*, 100−105.

(16) Majd, S. M.; Salimi, A.; Ghasemi, F. An ultrasensitive detection of miRNA-155 in breast cancer via direct hybridization assay using two-dimensional molybdenum disulfide field-effect transistor biosensor. *Biosens. Bioelectron.* **2018**, *105*, 6−13.

(17) Chen, S.; Sun, Y.; Xia, Y.; Lv, K.; Man, B.; Yang, C. Donor effect dominated molybdenum disulfide/graphene nanostructure-based field-effect transistor for ultrasensitive DNA detection. *Biosens. Bioelectron.* **2020**, *156*, 112128.

(18) Kashiwabara, T.; Takahashi, Y.; Tanimizu, M. A XAFS study on the mechanism of isotopic fractionation of molybdenum during its adsorption on ferromanganese oxides. *Geochem. J.* **2009**, *43*, e31−e36.

(19) Kashiwabara, T.; Takahashi, Y.; Tanimizu, M.; Usui, A. Molecular-scale mechanisms of distribution and isotopic fractionation of molybdenum between seawater and ferromanganese oxides. *Geochim. Cosmochim. Acta* **2011**, *75*, 5762−5784.

(20) Gustafsson, J. P.; Tiberg, C. Molybdenum binding to soil constituents in acid soils: An XAS and modelling study. *Chem. Geol.* **2015**, *417*, 279−288.

(21) Yang, S.; Uesugi, S.; Qin, H.; Tanaka, M.; Kurisu, M.; Miyamoto, C.; Kashiwabara, T.; Usui, A.; Takahashi, Y. Comparison of Arsenate and Molybdate Speciation in Hydrogenetic Ferromanganese Nodules. *ACS Earth and Space Chemistry* **2019**, *3*, 29−38.

(22) Schwarz, G. Molybdenum cofactor and human disease. *Curr. Opin. Chem. Biol.* **2016**, *31*, 179−187.

(23) Atwal, P. S.; Scaglia, F. Molybdenum cofactor deficiency. *Mol. Genet. Metab.* **2016**, *117*, 1−4.

https://doi.org/10.1021/acs.inorgchem.1c02600
Inorg. Chem. XXXX, XXX, XXX−XXX

(24) George, G. N.; Cleland, W. E.; Enemark, J. H.; Smith, B. E.; Kipke, C. A.; Roberts, S. A.; Cramer, S. P. L-Edge spectroscopy of molybdenum compounds and enzymes. *J. Am. Chem. Soc.* **1990**, *112*, 2541−2548.
(25) George, S. J.; Drury, O. B.; Fu, J.; Friedrich, S.; Doonan, C. J.; George, G. N.; White, J. M.; Young, C. G.; Cramer, S. P. Molybdenum X-ray absorption edges from 200 to 20,000 eV: The benefits of soft X-ray spectroscopy for chemical speciation. *J. Inorg. Biochem.* **2009**, *103*, 157−167.
(26) Rodriguez, J. A.; Chaturvedi, S.; Hanson, J. C.; Albornoz, A.; Brito, J. L. Electronic Properties and Phase Transformations in CoMoO4 and NiMoO4: XANES and Time-Resolved Synchrotron XRD Studies. *J. Phys. Chem. B* **1998**, *102*, 1347−1355.
(27) Izumi, Y.; Glaser, T.; Rose, K.; McMaster, J.; Basu, P.; Enemark, J. H.; Hedman, B.; Hodgson, K. O.; Solomon, E. I. Ligand K-Edge and Metal L-Edge X-ray Absorption Spectroscopy and Density Functional Calculations of Oxomolybdenum Complexes with Thiolate and Related Ligands: Implications for Sulfite Oxidase. *J. Am. Chem. Soc.* **1999**, *121*, 10035−10046.
(28) Bjornsson, R.; Delgado-Jaime, M. U.; Lima, F. A.; Sippel, D.; Schlesier, J.; Weyhermüller, T.; Einsle, O.; Neese, F.; DeBeer, S. Molybdenum L-Edge XAS Spectra of MoFe Nitrogenase. *Z. Anorg. Allg. Chem.* **2015**, *641*, 65−71.
(29) Bare, S. R.; Mitchell, G. E.; Maj, J. J.; Vrieland, G. E.; Gland, J. L. Local site symmetry of dispersed molybdenum oxide catalysts: XANES at the Mo L2,3-edges. *J. Phys. Chem.* **1993**, *97*, 6048−6053.
(30) Hu, H.; Wachs, I. E.; Bare, S. R. Surface Structures of Supported Molybdenum Oxide Catalysts: Characterization by Raman and Mo L3-Edge XANES. *J. Phys. Chem.* **1995**, *99*, 10897−10910.
(31) Aritani, H.; Tanaka, T.; Funabiki, T.; Yoshida, S.; Eda, K.; Sotani, N.; Kudo, M.; Hasegawa, S. Study of the Local Structure of Molybdenumâ'Magnesium Binary Oxides by Means of Mo L3-Edge XANES and UVâ'Vis Spectroscopy. *J. Phys. Chem.* **1996**, *100*, 19495−19501.
(32) Al Samarai, M.; Meirer, F.; Karunakaran, C.; Wang, J.; Vogt, E. T.; Zandbergen, H. W.; Weber, T.; Weckhuysen, B. M.; De Groot, F. M. Unraveling the redox behavior of a CoMoS hydrodesulfurization catalyst: A scanning transmission X-ray microscopy study in the tender X-ray range. *J. Phys. Chem. C* **2015**, *119*, 2530−2536.
(33) Surisetty, V. R.; Hu, Y.; Dalai, A. K.; Kozinski, J. Structural characterization and catalytic performance of alkali (K) and metal (Co and Rh)-promoted MoS2 catalysts for higher alcohols synthesis. *Appl. Catal., A* **2011**, *392*, 166−172.
(34) Lee, K. E.; Liu, L.; Kelly, T. L. Effect of Molybdenum Oxide Electronic Structure on Organic Photovoltaic Device Performance: An X-ray Absorption Spectroscopy Study. *J. Phys. Chem. C* **2014**, *118*, 27735−27741.
(35) Yao, K. P. C.; Risch, M.; Sayed, S. Y.; Lee, Y.-L.; Harding, J. R.; Grimaud, A.; Pour, N.; Xu, Z.; Zhou, J.; Mansour, A.; Bardé, F.; Shao-Horn, Y. Solid-state activation of Li2O2 oxidation kinetics and implications for Li-O2 batteries. *Energy Environ. Sci.* **2015**, *8*, 2417−2426.
(36) Najmi, S.; Rasmussen, M.; Innocenti, G.; Chang, C.; Stavitski, E.; Bare, S. R.; Medford, A. J.; Medlin, J. W.; Sievers, C. Pretreatment Effects on the Surface Chemistry of Small Oxygenates on Molybdenum Trioxide. *ACS Catal.* **2020**, *10*, 8187−8200.
(37) Zhang, H.; Lin, H.; Zheng, Y. Deactivation study of unsupported nano MoS2 catalyst. *Carbon Resources Conversion* **2020**, *3*, 60−66.
(38) Abedin, M. A.; Kanitkar, S.; Bhattar, S.; Spivey, J. J. Mo oxide supported on sulfated hafnia: Novel solid acid catalyst for direct activation of ethane & propane. *Appl. Catal., A* **2020**, *602*, 117696.
(39) Abedin, M. A.; Kanitkar, S.; Bhattar, S.; Spivey, J. J. Methane dehydroaromatization using Mo supported on sulfated zirconia catalyst: Effect of promoters. *Catal. Today* **2021**, *365*, 71−79.
(40) Vedachalam, S.; Boahene, P.; Dalai, A. K. Oxidative desulfurization of heavy gas oil over a Tiâ'TUD-1-supported Keggin-type molybdenum heteropolyacid. *Energy Fuels* **2020**, *34*, 15299−15312.
(41) Ramanathan, A.; Wu, J.-F.; Maheswari, R.; Hu, Y.; Subramaniam, B. Synthesis of molybdenum-incorporated mesoporous silicates by evaporation-induced self-assembly: Insights into surface oxide species and corresponding olefin metathesis activity. *Microporous Mesoporous Mater.* **2017**, *245*, 118−125.
(42) Uchagawkar, A.; Ramanathan, A.; Hu, Y.; Subramaniam, B. Highly dispersed molybdenum containing mesoporous silicate (Mo-TUD-1) for olefin metathesis. *Catal. Today* **2020**, *343*, 215−225.
(43) Radhakrishnan, R.; Reed, C.; Oyama, S. T.; Seman, M.; Kondo, J. N.; Domen, K.; Ohminami, Y.; Asakura, K. Variability in the Structure of Supported MoO 3 Catalysts: Studies Using Raman and X-ray Absorption Spectroscopy with ab Initio Calculations. *J. Phys. Chem. B* **2001**, *105*, 8519−8530.
(44) Zhang, H.; Lin, H.; Zheng, Y.; Hu, Y.; MacLennan, A. Understanding of the effect of synthesis temperature on the crystallization and activity of nano-MoS2 catalyst. *Appl. Catal., B* **2015**, *165*, 537−546.
(45) Bolanz, R. M.; Grauer, C.; Cooper, R. E.; Göttlicher, J.; Steininger, R.; Perry, S.; Küsel, K. Incorporation of molybdenum(vi) in akaganéite (*β*-FeOOH) and the microbial reduction of Mo-akaganéite by: Shewanella loihica PV-4. *CrystEngComm* **2017**, *19*, 6189−6198.
(46) Hämäläinen, K.; Siddons, D. P.; Hastings, J. B.; Berman, L. E. Elimination of the inner-shell lifetime broadening in x-ray-absorption spectroscopy. *Phys. Rev. Lett.* **1991**, *67*, 2850−2853.
(47) Glatzel, P.; De Groot, F. M.; Manoilova, O.; Grandjean, D.; Weckhuysen, B. M.; Bergmann, U.; Barrea, R. Range-extended EXAFS at the L edge of rare earths using high-energy-resolution fluorescence detection: A study of La in LaOCl. *Phys. Rev. B: Condens. Matter Mater. Phys.* **2005**, *72*, 014117.
(48) Glatzel, P.; Weng, T.-C.; Kvashnina, K.; Swarbrick, J.; Sikora, M.; Gallo, E.; Smolentsev, N.; Mori, R. A. Reflections on hard X-ray photon-in/photon-out spectroscopy for electronic structure studies. *J. Electron Spectrosc. Relat. Phenom.* **2013**, *188*, 17−25.
(49) Lafuerza, S.; Retegan, M.; Detlefs, B.; Chatterjee, R.; Yachandra, V.; Yano, J.; Glatzel, P. New reflections on hard X-ray photon-in/photon-out spectroscopy. *Nanoscale* **2020**, *12*, 16270−16284.
(50) de Groot, F. M.; Hu, Z. W.; Lopez, M. F.; Kaindl, G.; Guillot, F.; Tronc, M. Differences between L3 and L2 x-ray absorption spectra of transition metal compounds. *J. Chem. Phys.* **1994**, *101*, 6570−6576.
(51) Thomas, R.; Kas, J.; Glatzel, P.; Al Samarai, M.; de Groot, F. M. F.; Alonso Mori, R.; Kavčič, M.; Zitnik, M.; Bucar, K.; Rehr, J. J.; Tromp, M. Resonant Inelastic X-ray Scattering of Molybdenum Oxides and Sulfides. *J. Phys. Chem. C* **2015**, *119*, 2419.
(52) Lede, E. J.; Requejo, F. G.; Pawelec, B.; Fierro, J. L. G. XANES Mo L -Edges and XPS Study of Mo Loaded in HY Zeolite. *J. Phys. Chem. B* **2002**, *106*, 7824−7831.
(53) Alperovich, I.; Moonshiram, D.; Soldatov, A.; Pushkar, Y. Ru L2,3 XANES theoretical simulation with DFT: A test of the core-hole treatment. *Solid State Commun.* **2012**, *152*, 1880−1884.
(54) Alperovich, I.; Smolentsev, G.; Moonshiram, D.; Jurss, J. W.; Concepcion, J. J.; Meyer, T. J.; Soldatov, A.; Pushkar, Y. Understanding the Electronic Structure of 4d Metal Complexes: From Molecular Spinors to L-Edge Spectra of a di-Ru Catalyst. *J. Am. Chem. Soc.* **2011**, *133*, 15786−15794.
(55) Van Kuiken, B. E.; Valiev, M.; Daifuku, S. L.; Bannan, C.; Strader, M. L.; Cho, H.; Huse, N.; Schoenlein, R. W.; Govind, N.; Khalil, M. Simulating Ru L3-edge X-ray absorption spectroscopy with time-dependent density functional theory: Model complexes and electron localization in mixed-valence metal dimers. *J. Phys. Chem. A* **2013**, *117*, 4444−4454.
(56) Blaha, P.; Schwarz, K.; Madsen, G. K. H.; Kvasnicka, D.; Luitz, J. *WIEN2k, An Augmented Plane Wave + Local Orbitals Program for Calculating Crystal Properties*; Karlheinz Schwarz, Techn. Universität Wien: Wien, Austria, 2001.
(57) Bunău, O; Joly, Y Self-consistent aspects of x-ray absorption calculations. *J. Phys.: Condens. Matter* **2009**, *21*, 345501.

https://doi.org/10.1021/acs.inorgchem.1c02600
Inorg. Chem. XXXX, XXX, XXX−XXX

(58) Rovezzi, M.; et al. TEXS: in-vacuum tender X-ray emission spectrometer with 11 Johansson crystal analyzers. *J. Synchrotron Radiat.* **2020**, *27*, 813−826.
(59) Carra, P.; Fabrizio, M.; Thole, B. T. High resolution x-ray resonant Raman scattering. *Phys. Rev. Lett.* **1995**, *74*, 3700−3703.
(60) de Groot, F. M. F.; Krisch, M. H.; Vogel, J. Spectral sharpening of the Pt L edges by high-resolution x-ray emission. *Phys. Rev. B: Condens. Matter Mater. Phys.* **2002**, *66*, 195112.
(61) Campbell, J.; Papp, T. Widths of the atomic K-N7 levels. *At. Data Nucl. Data Tables* **2001**, *77*, 1−56.
(62) Duscher, G.; Buczko, R.; Pennycook, S.; Pantelides, S. Core-hole effects on energy-loss near-edge structure. *Ultramicroscopy* **2001**, *86*, 355−362.
(63) Hébert, C. Practical aspects of running the WIEN2k code for electron spectroscopy. *Micron* **2007**, *38*, 12−28.
(64) Manyakin, M. D.; Kurganskii, S. I.; Dubrovskii, O. I.; Chuvenkova, O. A.; Domashevskaya, E. P.; Turishchev, S. Y. Ab initio calculation and synchrotron X-ray spectroscopy investigations of tin oxides near the Sn L 3 absorption edges. *Phys. Solid State* **2016**, *58*, 2379−2384.
(65) Hedman, B.; Penner-Hahn, J. E.; Hodgson, K. O. In *EXAFS and Near Edge Structure III. Springer Proceedings in Physics*, Vol. *2*.; Hodgson, K. O., Hedman, B., Penner-Hahn, J. E., Eds.; Springer: Berlin, Heidelberg, 1984; pp 64−66.
(66) Choi, J.-G.; Thompson, L. XPS study of as-prepared and reduced molybdenum oxides. *Appl. Surf. Sci.* **1996**, *93*, 143−149.
(67) Theil, C.; van Elp, J.; Folkmann, F. Ligand field parameters obtained from and chemical shifts observed at the Cr L2,3 edges. *Phys. Rev. B: Condens. Matter Mater. Phys.* **1999**, *59*, 7931−7936.
(68) Sasaki, T. A.; Kiuchi, K. Electronic structures and X-ray photoelectron spectra of MoO2 and Li2MoO4. *Chem. Phys. Lett.* **1981**, *84*, 356−360.
(69) Hölzer, G.; Fritsch, M.; Deutsch, M.; Härtwig, J.; Förster, E. Kα1,2 and Kβ1,3 x-ray emission lines of the 3d transition metals. *Phys. Rev. A: At., Mol., Opt. Phys.* **1997**, *56*, 4554−4568.
(70) Asakura, H.; Shishido, T.; Yamazoe, S.; Teramura, K.; Tanaka, T. Structural analysis of group V, VI, and VII metal compounds by XAFS. *J. Phys. Chem. C* **2011**, *115*, 23653−23663.
(71) Newman, D. J., Ng, B., Eds. *Crystal Field Handbook*; Cambridge University Press: 2000.
(72) Hedman, B.; Frank, P.; Gheller, S. F.; Roe, A. L.; Newton, W. E.; Hodgson, K. O. New structural insights into the iron-molybdenum cofactor from Azotobacter vinelandii nitrogenase through sulfur K and molybdenum L x-ray absorption edge studies. *J. Am. Chem. Soc.* **1988**, *110*, 3798−3805.
(73) Eyert, V.; Horny, R.; Höck, K. H.; Horn, S. Embedded Peierls instability and the electronic structure of MoO2. *J. Phys.: Condens. Matter* **2000**, *12*, 4923−4946.

https://doi.org/10.1021/acs.inorgchem.1c02600
Inorg. Chem. XXXX, XXX, XXX−XXX